The *Hubble Space Telescope* UV Legacy Survey of Galactic Globular Clusters - XVII. Public Catalogue Release.∗†

D. Nardiello[1,2]‡, M. Libralato[3], G. Piotto[1,2], J. Anderson[3], A. Bellini[3],
A. Aparicio[4,5], L. R. Bedin[2], S. Cassisi[6], V. Granata[1,2], I. R. King[7], F. Lucertini[1],
A. F. Marino[8], A. P. Milone[1], S. Ortolani[1], I. Platais[9], R. P. van der Marel[3,9]

[1]*Dipartimento di Fisica e Astronomia "Galileo Galilei", Università di Padova, Vicolo dell'Osservatorio 3, Padova IT-35122*
[2]*Istituto Nazionale di Astrofisica - Osservatorio Astronomico di Padova, Vicolo dell'Osservatorio 5, Padova, IT-35122*
[3]*Space Telescope Science Institute, 3800 San Martin Drive, Baltimore, MD 21218, USA*
[4]*Instituto de Astrofisica de Canarias, E-38200 La Laguna, Tenerife, Canary Islands, Spain*
[5]*Department of Astrophysics, University of La Laguna, E-38200 La Laguna, Tenerife, Canary Islands, Spain*
[6]*Osservatorio Astronomico d'Abruzzo, Via M. Maggini sn., I-64100 Teramo, Italy*
[7]*Department of Astronomy, University of Washington, Box 351580, Seattle, WA 98195, USA*
[8]*Research School of Astronomy and Astrophysics, The Australian National University, Cotter Road, Weston, ACT, 2611, Australia*
[9]*Center for Astrophysical Sciences, Department of Physics & Astronomy, Johns Hopkins University, Baltimore, MD 21218, USA*

ABSTRACT

In this paper we present the astro-photometric catalogues of 56 globular clusters and one open cluster. Astrometry and photometry are mainly based on images collected within the "HST Legacy Survey of Galactic Globular Clusters: Shedding UV Light on Their Populations and Formation" (GO-13297, PI: Piotto), and the "ACS Survey of Galactic Globular Clusters" (GO-10775, PI: Sarajedini). For each source in the catalogues for which we have reliable proper motion we also publish a membership probability for separation of field and cluster stars. These new catalogues, which we make public in Mikulski Archive for Space Telescopes, replace previous catalogues by Paper VIII of this series.

Key words: globular clusters: general – Hertzsprung-Russell and colour-magnitude diagrams – stars: Population II – techniques: photometric – catalogues

1 INTRODUCTION

Nowadays the presence of multiple stellar populations (MPs) in globular clusters (GCs) is a commonly accepted observational fact, even though our understanding of their origin is still far from satisfying (Renzini et al. 2015; Bastian 2015, Bastian & Lardo 2018). The "HST Legacy Survey of Galactic Globular Clusters: Shedding UV Light on Their Populations and Formation" (GO-13297, PI: Piotto) observations, combined with the optical data from the "ACS Survey of Galactic Globular Clusters" (ACS GCS; GO-10775,

PI: Sarajedini) have provided key building blocks for the observational edifice of MPs. These datasets have allowed us to demonstrate their ubiquitous presence in all Galactic GCs studied in enough details, convincingly showing the existence of discrete populations, establishing a tight connection between photometric and spectroscopic data, and spurring further studies by discovering populations with particularly complex chemical patterns (Piotto et al. 2015, hereafter Paper I; Milone et al. 2017; Marino et al. 2018 and references therein).

In this paper, we present and publish the final catalogues. These catalogues contain astrometric positions, F275W, F336W, F438W, F606W, and F814W photometry and cluster membership from proper motions (PMs) of stars in the central regions of 56 GCs and the old super metal-rich open cluster (OC) NGC 6791, presented in Paper I. The GO-13297 data are complemented here by the Wide Field Camera 3 (WFC3) images collected within the GO-12311 (PI: Piotto) and GO-12605 (PI: Piotto) programs, used as

pilot projects for the more extended UV Legacy survey. As discussed in Section 5, the catalogues presented in this paper replace our preliminary catalogues published by Soto et al. (2017, Paper VIII). The complete GO-13297 dataset also includes the astrometry and photometry catalogues of the external fields taken with the Advanced Camera for Surveys (ACS), in parallel with the GO-13297 WFC3/UVIS central fields and published by Simioni et al. (2018, Paper XIII).

The paper is organised as follows. Section 2 is dedicated to the observations and data reduction; section 3 briefly presents the colour-magnitude diagrams; the proper motion measurements and the methodology to estimate membership probability are described in section 4. Section 5 discusses the improvements of the new data reduction with respect to the preliminary one of Paper VIII. In section 6 we describe the content of the data release tables.

2   OBSERVATIONS AND DATA REDUCTION

In this paper, we present high-precision stellar astrometry and photometry from WFC3/UVIS and ACS/WFC observations of 56 GCs and the old open cluster NGC 6791. The GCs were all observed with ACS/WFC in F606W and F814W bands within GO-10775 (PI: A. Sarajedini). For the open cluster NGC 6791 we used the ACS/WFC data in the same filters collected within GO-10265 (PI: T. Brown). Observations in the UV/blue *HST* bands (F275W, F336W, and F438W) of 55 clusters were collected with the WFC3/UVIS camera within GO-12311 (PI: G. Piotto), GO-12605 (PI: G. Piotto) , and GO-13297 (PI: G. Piotto) programs. A complete log of these observations is presented in Paper I. In addition to the data used in Paper I, for NGC 0104 we also incorporated F336W observations from GO-11729 (PI: J. Holtzman) and GO-12971 (PI: H. Richer), and F435W images collected with ACS/WFC within GO-9443 (PI: I. King) and GO-9281 (PI: J. Grindlay). For NGC 6752 we used F275W data from GO-12311, F336W images from GO-11729, and F435W ACS/WFC observations obtained by GO-12254 (PI: A. Cool).

2.1   First-pass photometry

We worked on `_flc` images, which are `_flt` exposures corrected for charge-transfer efficiency (CTE) defects (Anderson & Bedin 2010). For the data reduction we used an evolution of the software described in Anderson et al. (2008). A detailed description of the adopted tools is given by Bellini et al. (2017), Nardiello et al. (2018), and Libralato et al. (2018).

Briefly, for each image, we accounted on the spatial and time dependence of the Point Spread Function (PSF) by constructing an optimal PSF for each exposure by perturbing the "library" PSF[1] appropriate for each filter. In order to obtain the perturbed PSFs we used the FORTRAN program `hst1pass` (see also Bellini et al. 2018); we selected bright, unsaturated, isolated stars, we measured the flux and the positions using the library PSFs, and finally we subtracted a model of each star to the real star. The residuals of the
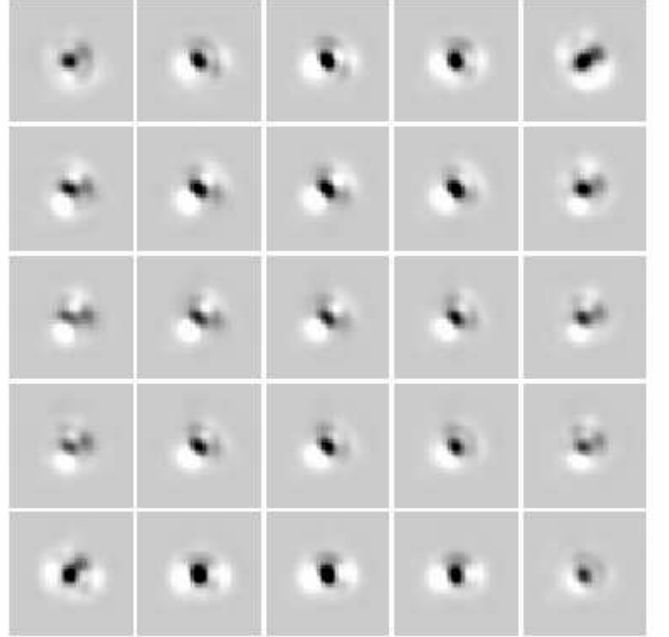
---

[1] http://www.stsci.edu/~jayander/STDPSFs/

Figure 1. A 5 × 5 grid of perturbation PSFs that modify the library PSF array in the case of the image `j9l959f6q` (NGC 6352). The total variation across the the grid goes from ~ −2% to ~ 1% of the star's total flux.

subtraction are averaged to form a grid of residuals used to perturb the library PSFs. This grid has dimensions that go from 1 × 1 to 5 × 5, depending on the total number of stars available in the field. Each element of the grid corresponds to a different fiducial location on the detector, and we used linear interpolation to evaluate the PSF between these locations. Nine rounds of iterations allowed us to arrive at an evenly spaced set of perturbation PSFs from the random distribution of stars in each image. An example of the grid of residual PSFs is shown in Fig. 1.

With these arrays of PSFs, we extracted the preliminary catalogues using the program `hst1pass`. This program measures positions and fluxes of the stars on the single HST exposures, without performing any neighbour subtraction. It is even able to make measurements of saturated stars, using the technique described in Gilliland (2004) and Gilliland et al. (2010). We corrected the positions of the stars for geometric distortion using the routines described in Anderson & King (2006, ACS/WFC), and Bellini & Bedin (2009), Bellini et al. (2011, WFC3/UVIS).

We transformed all the catalogues into a common reference system. We adopted the *Gaia* Data Release 1 catalogue (Gaia Collaboration et al. 2016b) as the reference system for positions. In this way, the X- and Y-axes are aligned with West and North, respectively. We de-projected the *Gaia* (α, δ)-coordinates onto a tangent plane with the cluster centre from Goldsbury et al. (2010) as the tangent point (α_0, δ_0). We transformed these coordinates into WFC3/UVIS pixels (pixel scale 0.0395 arcsec pixel^{-1}; Dressel 2018), positioning the centre of the cluster in the pixel (5000,5000). In the first iteration, we found the six-parameter linear transformations between this master catalogue and each of the

single-exposure catalogues by using unsaturated, bright, and isolated stars, and used this transformation to transform all stars measured in each exposure into this reference frame. We collated these lists and extracted a new master catalogue with the 3σ-clipped average stellar positions. We then used this new catalogue to improve the transformations, iterating until the precision on the transformed positions did not improve. For each filter, the photometric zero-point of each individual catalogue is tied to those of the deepest exposure. For each filter, we obtained a final catalogue containing the 3σ-clipped average stellar positions and magnitudes in that filter ("first-pass" photometry, similar to that used in Paper I).

2.2 Multiple-pass photometry

In the "multiple-pass" photometry stage, we used the images, the PSF arrays and the transformations obtained during the "first-pass" to simultaneously find and measure stars in all the individual exposures. The tool we used is the FORTRAN software kitchen_sync2 (KS2; Bellini et al. 2017; Nardiello et al. 2018; Libralato et al. 2018). The software analyses all the images simultaneously to find and measure the sources; in this way it is able to also measure the stars that cannot be detected in individual exposures. To avoid spurious detection caused by artifacts of the PSF, and in order to detect faint stars close to bright stars, KS2 creates an ad-hoc mask for bright and saturated stars, which were included in the one-pass catalogues.

The finding procedure is accomplished through different iterations. During the first iteration, the software identifies the bright stars and subtracts them. In the following step, the routine searches for stars that are fainter than the stars from previous iteration and then measures and subtracts them. In each iteration we defined different criteria (which are increasingly more relaxed from the first to the last iteration) to qualify a source as a star. We chose to iterate 8 times: in the first five iterations we required that a stars be present both in the F606W and F814W exposures; in iteration six, seven, and eight we performed the finding on the F275W, F336W, and F438W exposures to detect the stars that are brighter in the UV/blue filters than optical filters (i.e., white dwarfs) and not detected in optical filters.

The KS2 software generated astrometric and photometric catalogues of stars using three different methods. A detailed description of the three methods is given in Bellini et al. (2017).

Method-1 gives the best results for stars that are bright enough to generate star-like profiles in individual exposures. During the finding stage, the routine searches for a distinct peak in a 5×5 pixel^2 raster and measures, in each image, the flux and the position of the source using an appropriate local PSF, after subtracting the neighbour stars. The local sky value is computed inside an annulus with an inner radius $r_{\rm in} = 4$ pixels and outer radius $r_{\rm out} = 8$ pixels. The final flux and position of a star in a filter is given by a robust average of the fluxes and positions measured in the single exposures.

Method-2 works well for faint stars and crowded environments. Starting from the position obtained during the finding stage, KS2 performs weighted aperture photometry of the star in a raster of 5×5 pixels, after neighbour-subtraction; each pixel is weighted in such a way that pixel containing neighbour stars are down-weighted. The local sky is computed as above for method-1. The final flux is a robust average of the fluxes obtained in the single exposures.

Method-3 works well in very crowded environments. It is similar to method-2, but uses only the pixels inside a radius $r = 0.75$ pixel from the centre of the star and the sky is calculated in a tight annulus with $r_{\rm in} = 2$ pixels and $r_{\rm out} = 4$ pixels.

Saturated stars are not measured by KS2. They were, however, included in the one-pass based catalogues using techniques described above.

In addition to the astro-photometric catalogue, KS2 also outputs stacked versions of the fields obtained from the _flc images. Excluding NGC 0104, NGC 6752, and NGC 5897, for all the clusters we generated 7 different stacked images: one for the filters F275W, F336W, and F438W, and two for the filters F606W and F814W, separating short- and long-exposure images. For NGC 5897 the F814W short-exposure image is unusable. For NGC 0104 and NGC 6752 we generated 8 stacked images: one for the filters F275W and F336W, and two for the filters F435W, F606W and F814W, one for short-exposure observations and one for the long ones.

2.3 Photometric Calibration

We calibrated the output photometry from KS2 into the Vega-mag system by comparing aperture photometry on _drc images (which are normalised to the exposure time of 1 s) with our PSF-based photometry.

For aperture photometry on _drc images we used an aperture radius $r_{\rm AP} = 0.2$ arcsec. We adopted the $r_{\rm AP}$ after testing different apertures (from 0.04 arcsec to 0.4 arcsec) on a sample of 10 GCs images with different crowding level and total number of stars. We found that $r_{\rm AP} = 0.2$ arcsec gives, on average, the lowest error on the determination of the zeropoint that converts the instrumental magnitudes to calibrated magnitudes. It represents a fair compromise between measuring as much flux as possible for the stars ($\gtrsim 80\%$) on the _drc images and avoiding the contamination from neighbour stars.

We corrected the aperture photometry magnitudes $m_{\rm AP}^{\rm drc}$ with the appropriate aperture correction[2], obtaining the magnitudes for an infinite-aperture radius $m_{\rm AP,\infty}^{\rm drc}$.

For each filter we cross-identified the stars in common between the catalogue obtained using KS2 and that obtained from aperture photometry on _drc images, and computed the 3σ-clipped average $< \delta m >$, and the associated error, of the difference $\delta m = m_{\rm AP,\infty}^{\rm drc} - m_{\rm PSF}^{flc}$, where $m_{\rm PSF}^{flc}$ is the magnitude associated with the PSF photometry on _flc images output of KS2.

The calibrated magnitude $m_{\rm CAL,X}$ of a star in the filter X is given by:

$$m_{\rm CAL,X} = m_{\rm PSF,X}^{flc} + < \delta m > + {\rm ZP_X} \tag{1}$$

where ${\rm ZP_X}$ is the zero-point associated with filter X. We

---

[2] For ACS we used the aperture correction tabulated by Bohlin (2016), while for WFC3 we used the corrections in Deustua et al. (2017)

Table 1. Difference between $m_{\mathrm{CAL,X}}$ and $m_{\mathrm{PSF,X}}^{flc}$ for each filter X

Cluster	F275W	F336W	F438W[1]	F606W	F814W
NGC 0104	28.75±0.04	30.42±0.02	30.71±0.01	30.60±0.03	29.70±0.03
NGC 0288	28.94±0.01	29.66±0.01	28.85±0.01	31.62±0.01	30.88±0.01
NGC 0362	29.19±0.04	29.66±0.02	29.14±0.01	31.80±0.02	31.04±0.02
NGC 1261	29.75±0.02	29.84±0.01	30.38±0.01	32.71±0.02	31.85±0.02
NGC 1851	30.21±0.02	29.94±0.01	30.18±0.01	32.71±0.02	31.82±0.02
NGC 2298	30.34±0.03	29.66±0.01	30.14±0.01	32.71±0.02	31.82±0.02
NGC 2808	29.89±0.02	30.33±0.02	29.77±0.02	32.74±0.03	31.87±0.05
NGC 3201	29.62±0.01	29.53±0.01	29.39±0.01	31.35±0.01	30.46±0.02
NGC 4590	29.53±0.01	29.51±0.01	29.26±0.01	31.64±0.02	30.89±0.02
NGC 4833	29.85±0.01	29.66±0.01	30.15±0.01	31.78±0.01	31.03±0.01
NGC 5024	30.58±0.01	29.96±0.01	30.46±0.01	32.68±0.03	31.78±0.03
NGC 5053	29.74±0.03	29.84±0.01	30.34±0.01	32.68±0.01	31.82±0.02
NGC 5272	28.96±0.02	29.66±0.02	28.87±0.01	31.64±0.02	30.90±0.03
NGC 5286	29.66±0.02	29.56±0.02	29.33±0.01	32.71±0.03	31.85±0.03
NGC 5466	30.14±0.03	29.65±0.01	30.13±0.01	32.69±0.02	31.82±0.02
NGC 5897	29.84±0.01	29.65±0.01	30.18±0.01	32.68±0.02	31.82±0.02
NGC 5904	29.51±0.01	29.51±0.01	29.22±0.01	31.71±0.02	30.82±0.02
NGC 5927	29.58±0.04	29.51±0.01	29.80±0.02	32.71±0.02	31.85±0.02
NGC 5986	29.61±0.01	29.49±0.01	29.33±0.01	32.72±0.02	31.82±0.03
NGC 6093	29.78±0.02	30.31±0.02	29.60±0.01	32.69±0.03	31.79±0.03
NGC 6101	29.86±0.01	29.84±0.01	30.35±0.01	32.77±0.02	31.91±0.02
NGC 6121	29.70±0.01	29.49±0.01	29.36±0.01	29.84±0.02	29.14±0.02
NGC 6144	29.63±0.02	29.51±0.01	29.28±0.01	32.68±0.01	31.82±0.02
NGC 6171	30.13±0.04	29.65±0.01	30.17±0.01	31.64±0.02	30.90±0.02
NGC 6205	29.00±0.02	29.66±0.01	28.97±0.01	31.72±0.03	30.83±0.03
NGC 6218	29.67±0.01	29.51±0.01	29.36±0.01	31.24±0.02	30.34±0.02
NGC 6254	29.68±0.01	29.51±0.01	29.37±0.01	31.23±0.02	30.34±0.02
NGC 6304	29.55±0.03	29.51±0.02	29.28±0.01	32.68±0.02	31.82±0.02
NGC 6341	29.55±0.02	29.51±0.02	29.24±0.02	31.72±0.02	30.90±0.03
NGC 6352	29.58±0.02	29.53±0.01	29.22±0.01	31.72±0.02	30.90±0.02
NGC 6362	29.58±0.02	29.57±0.01	29.40±0.01	31.64±0.01	30.90±0.02
NGC 6366	29.73±0.05	29.51±0.02	29.29±0.01	31.72±0.02	30.83±0.02
NGC 6388	30.16±0.03	29.65±0.05	30.11±0.02	32.68±0.05	31.81±0.06
NGC 6397	29.63±0.01	29.53±0.01	29.36±0.01	29.29±0.02	28.40±0.02
NGC 6441	30.29±0.07	29.64±0.04	30.06±0.02	32.68±0.05	31.81±0.06
NGC 6496	29.67±0.07	29.50±0.01	29.47±0.01	32.68±0.02	31.82±0.02
NGC 6535	29.68±0.03	29.51±0.01	29.30±0.01	31.64±0.01	30.90±0.02
NGC 6541	29.63±0.02	29.50±0.02	29.36±0.02	31.72±0.02	30.90±0.03
NGC 6584	29.55±0.03	29.53±0.01	29.29±0.01	32.72±0.02	31.85±0.02
NGC 6624	29.67±0.03	29.48±0.02	29.58±0.01	32.71±0.02	31.81±0.02
NGC 6637	29.86±0.02	29.66±0.01	30.10±0.01	32.68±0.02	31.78±0.02
NGC 6652	29.67±0.05	29.53±0.01	29.65±0.01	32.68±0.02	31.79±0.02
NGC 6656	29.69±0.02	29.99±0.01	30.19±0.01	30.70±0.02	29.99±0.02
NGC 6681	29.69±0.01	29.48±0.01	29.62±0.01	31.72±0.02	30.90±0.02
NGC 6715	30.51±0.03	29.97±0.04	30.51±0.02	32.69±0.04	31.82±0.04
NGC 6717	29.51±0.01	29.54±0.01	29.26±0.01	31.63±0.02	30.90±0.02
NGC 6723	29.59±0.02	29.54±0.01	29.27±0.01	31.73±0.02	30.91±0.02
NGC 6752	28.84±0.02	30.05±0.02	32.14±0.01	30.21±0.02	29.46±0.02
NGC 6779	29.69±0.01	29.47±0.01	29.58±0.01	32.68±0.02	31.82±0.02
NGC 6791	29.49±0.05	29.48±0.01	29.45±0.01	30.60±0.01	29.72±0.01
NGC 6809	29.71±0.01	29.47±0.01	29.36±0.01	30.97±0.02	30.22±0.02
NGC 6838	29.68±0.02	29.50±0.01	29.35±0.01	31.04±0.02	30.21±0.02
NGC 6934	29.67±0.02	29.50±0.01	29.42±0.01	32.69±0.02	31.79±0.02
NGC 6981	29.55±0.02	29.51±0.01	29.43±0.01	31.64±0.02	30.91±0.02
NGC 7078	29.53±0.02	29.65±0.02	29.34±0.01	31.64±0.03	30.90±0.04
NGC 7089	29.68±0.02	29.54±0.02	29.29±0.02	32.69±0.03	31.79±0.04
NGC 7099	29.58±0.02	29.50±0.01	29.35±0.01	31.72±0.02	30.82±0.02

[1] For NGC 0104 and NGC 6752, the value is referred to ACS/WFC F435W filter.

have obtained ZP_X for ACS/WFC using the "ACS Zero-points calculator"[3]; for WFC3/UVIS we adopted the zero-points tabulated by Deustua et al. (2017).

Table 1 contains the values of $< \delta m > + ZP_X$ and the associated errors for each cluster and for each filter.

2.4 Astrometric solution

As described in Section 2.1, our reference frame was based on the *Gaia* Data Release 1 catalogue (Gaia Collaboration et al. 2016b), which enables us to transform the coordinates from (X,Y) into (α, δ). As such, the positions are given for Equinox J2000 and referred to the epoch of *Gaia* observations (2015.0).

2.5 Quality parameters

In addition to the photometric error (RMS), the KS2 routine provides as output some quality parameters that are useful for selecting the best measured stars for a particular science case.

Among them, there is the quality-of-fit (QFIT) parameter that gives information about the goodness of the PSF-fitting during the measurement of the position and the flux of a star. It allows us to distinguish between stars and other sources (of astrophysical nature or not, e.g., cosmic rays, hot pixels, extended sources, etc). This parameter is computed using all the pixels of the raster where the source is measured (pixd), and pixels with neighbour stars are down-weighted. It is simply the linear-correlation coefficient between the observed and modelled pixels and is given by:

$$\text{QFIT} = \frac{\sum_{i,j} \text{pixd}(i,j)\,\text{PSF}(i,j)}{\sqrt{\sum_{i,j} \text{PSF}^2(i,j) \sum_{i,j} \text{pixd}^2(i,j)}} \qquad (2)$$

where the sum is performed on a 5×5 pixel^2 raster pixd (after neighbour subtraction) centred on the target stars, and PSF(i,j) is the value of the local PSF-model expected in the pixel (i,j).

Introduced by Bedin et al. (2008, see also Bedin et al. 2009, 2010; Simioni et al. 2018), the parameter RADXS is a shape parameter that allows us to distinguish sources that deviate from a PSF shape. It is a comparison between the measured flux of the source outside the core (in an annulus $1.0 < r < 2.5$ pixels) and the flux expected from the PSF-model. For RADXS>0 the source is broader than that expected from the model (i.e., galaxies), while for negative values of RADXS the source is sharper than the PSF (i.e., cosmic rays and artifacts).

Finally, the KS2 routine gives the number of images in which a star is found (N_f) and the number of consistent measurements of the star used to compute its average position and flux (N_g).

[3] https://acszeropoints.stsci.edu/

3 COLOUR-MAGNITUDE DIAGRAMS

In Fig. 2 we show an example of selection of well-measured stars for the case of NGC 6752 and the photometric method-1. Similar plots can be made for the methods 2 and 3. The top and middle panels of Fig. 2 show the selection of the stars based on the distribution of the photometric errors (RMS, left-hand panels), the quality of fit (QFIT, center panels), and the shape of the sources (RADXS, right-hand panels), in the case of F275W (top panels) and F336W (middle panels) filters. The selection based on RMS and QFIT are performed as done by Milone et al. (2012): we divided the distributions in 12 magnitude bins and, in each bin, we calculated the 3.5σ-clipped average of the magnitude and of the parameter, where σ is the standard deviation associated to the average value in the given bin. We added to the mean parameter of each bin $3.5 \times \sigma$, and we linearly interpolated these points (green line). We excluded all the points above (in the case of the RMS) or below (in the case of the QFIT) the green line (azure points). For the sharp parameter, we selected all the stars that satisfy the condition: $-0.15 <$RADXS$< +0.15$. Bottom panels show the m_{F275W} versus $(m_{F275W} - m_{F336W})$ colour-magnitude diagram (CMD) for the stars that pass the selection criteria in both filters (left-hand panel) and for the stars that were rejected in at least one filter (right-hand panel). In red, the stars that are saturated in at least one filter and that have been recovered from the "first-pass" photometry. From the CMDs, it is clear that many stars with poor photometric quality are rejected

Figure 3 shows a comparison of the CMDs of NGC 6752 obtained using the three photometric methods described in Sect. 2: top-panels show the m_{F275W} versus $(m_{F275W} - m_{F336W})$ CMDs of NGC 6752 in the bright regime of magnitudes $(16.5 < m_{F275W} < 20.5)$ and obtained with method-1 (panel (a_1)), method-2 (panel (a_2)), and method-3 (panel (a_3)). The middle panels (b_1), (b_2), and (b_3) of Fig. 3 show the same CMDs for stars with $22.0 < m_{F275W} < 26.9$. The stars plotted in the CMDs have passed the selection criteria above described applied to each photometric method. Top panels show that for bright stars method-1 gives better results than method-2 and method-3. Panel (b_1) shows that method-1 gives a good measurement of the stars with $m_{F275W} \lesssim 23.0$; stars having magnitude $23.0 \lesssim m_{F275W} \lesssim 25.5$ are well measured with method-2, while method-3 is an optimal choice for stars having $25.5 \lesssim m_{F275W} \lesssim 27.0$. Panel (c) of Fig. 3 shows the $m_{F275W} - m_{F336W}$ colour RMS as a function of the F275W magnitude: light red, light green, and light blue points are the RMS of the stars measured with method-1, method-2, and method-3, respectively. We divided the RMS distribution in bins of width 1 F275W magnitude, and we computed in each bin the median RMS. The binned RMS distributions of the three methods (in red, green, and blue for methods 1, 2, and 3, respectively), confirm that method-1 gives the best results in the bright magnitude regime, while stars measured with methods-2 and 3 have lower RMS at fainter magnitudes.

4 RELATIVE PROPER MOTIONS AND CLUSTER MEMBERSHIP PROBABILITIES

The photometric catalogs published with this manuscript are obtained with reduction pipelines fine tuned to achieve
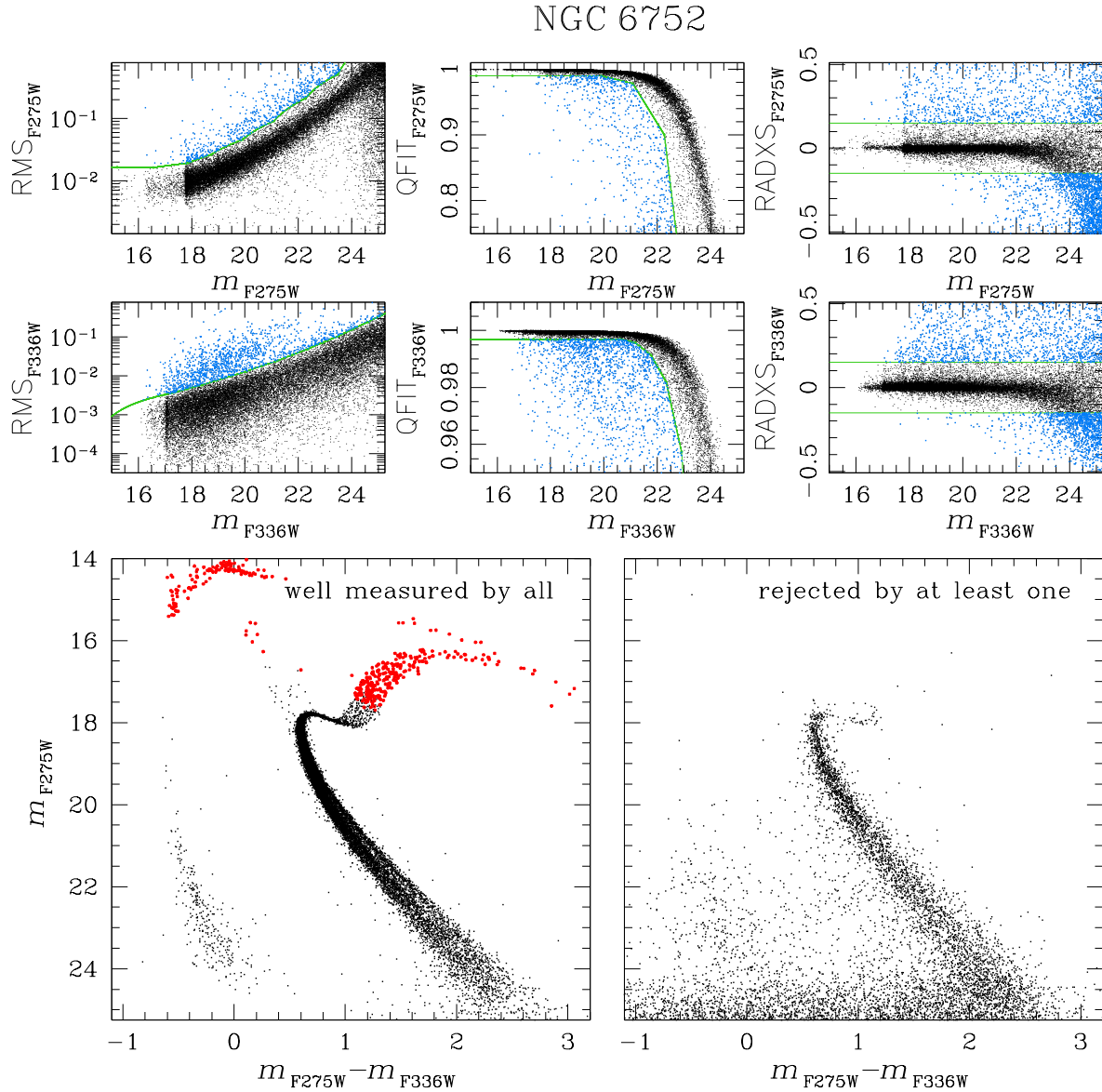
NGC 6752

Figure 2. Procedure adopted for selecting well-measured stars in the cluster NGC 6752. Top and middle panels show the selection of the stars based on RMS (left-hand panels), QFIT (central panels), and RADXS (right-hand panels) parameters: in azure the stars that are rejected. Bottom panels show the m_{F275W} versus ($m_{F275W} - m_{F336W}$) CMD cleaned by rejected stars in both filters (left-hand panel) and the CMD of the stars rejected in at least one filter. Red dots correspond to the stars that are saturated in at least one filter.

high-precision photometric measurements. High-precision proper motions require a completely different, ad-hoc reduction of the images (see, e.g., Bellini et al. 2014, 2018; Libralato et al. 2018), which is beyond the scope of the present manuscript. High-precision astrometry have different demands with respect to high-precision photometry since, to the first order, photometry cares of sum of pixels while astrometry is focused on differences between pixels. There are several systematic effects (e.g., CTE correction residuals, geometric-distortion correction residuals, color terms in the blue filters of the WFC3/UVIS, etc.) that cannot be properly accounted for with a reduction fine-tuned for photometry. These systematic effects can be as large as 0.2 ACS/WFC pixels in a given data set. The proper mo-

tions we computed for this work are based on image pairs, are insensitive to systematic errors, and are highly degenerate in terms of proper motion errors.

In summary, the present proper motions can be only used to calculate cluster membership in order to separate cluster members and field stars. We are presently working on the much more precise astrometry needed for internal kinematics ($\ll$0.1 mas/yr, see, e.g. Libralato et al. 2018), and we defer the publication of proper motions catalogues to future papers.

Selecting bona-fide cluster members by relying solely on the stellar positions on a CMD is not an easy task, in particular for those GCs near the Galactic plane or bulge. In principle, the user can combine our photome-
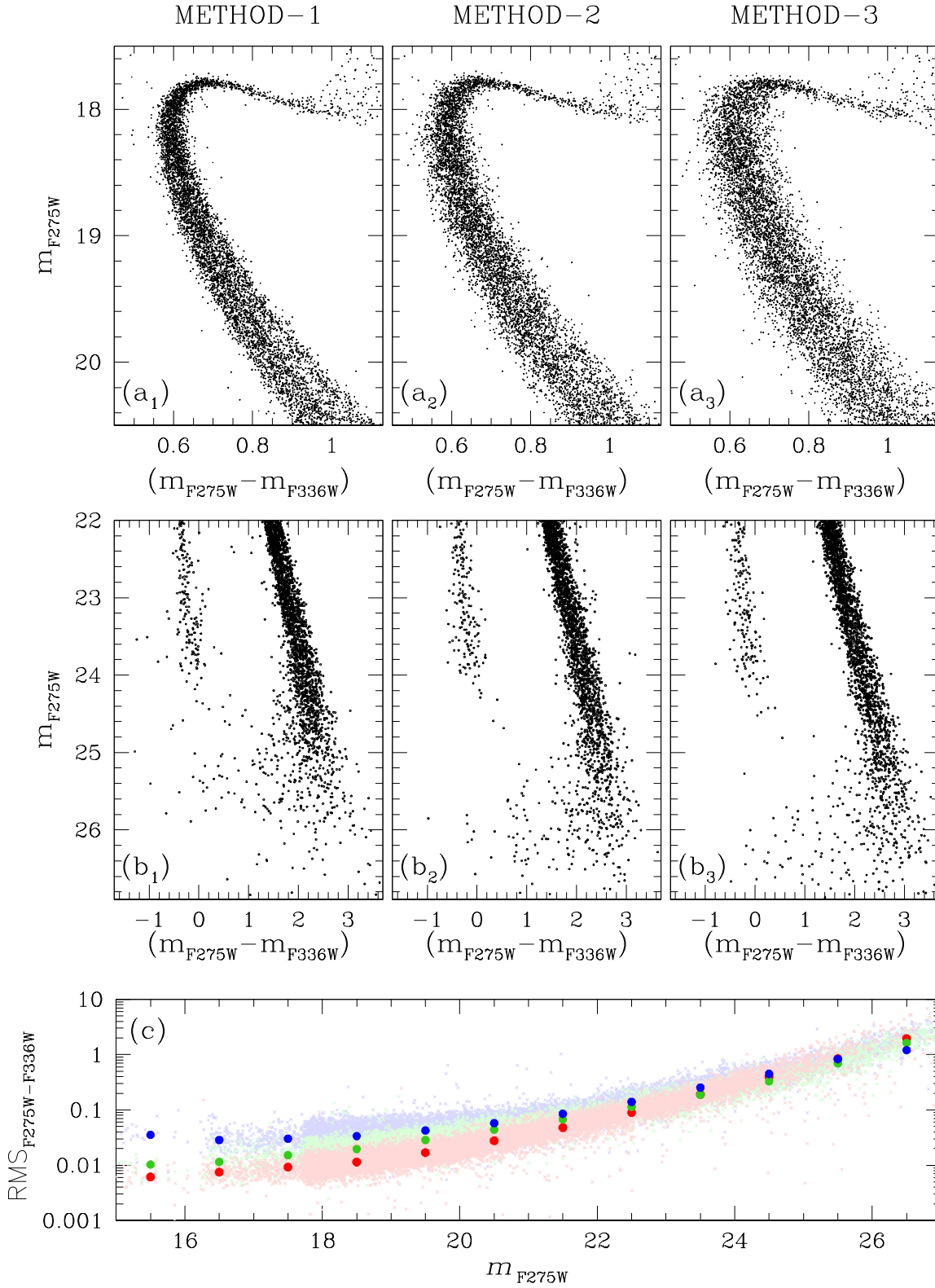
NGC 6752

METHOD−1   METHOD−2   METHOD−3

Figure 3. The CMDs of NGC 6752 obtained using the three photometric methods described in Sect. 2: top-panels show the m_{F275W} versus $(m_{F275W} - m_{F336W})$ CMDs for stars with $16.5 < m_{F275W} < 20.5$ and obtained with method-1 (panel (a_1)), method-2 (panel (a_2)), and method-3 (panel (a_3)). Middle panels (b_1), (b_2), and (b_3) show the same CMDs for stars with $22.0 < m_{F275W} < 26.9$. Panel (c) shows the colour RMS as a function of the F275W magnitude for the three photometric methods: in red the Method-1, in green the Method-2, and in blue the Method-3.

Table 2. Epochs of observations

Cluster	1st epoch	2nd epoch	Δt (yrs)	Cluster	1st epoch	2nd epoch	Δt (yrs)
NGC0104	2006.20	2013.14	6.94	NGC6352	2006.27	2014.01	7.74
NGC0288	2006.56	2012.83	6.27	NGC6362	2006.41	2014.37	7.96
NGC0362	2006.42	2012.70	6.28	NGC6366	2006.25	2014.50	8.25
NGC1261	2006.19	2013.93	7.74	NGC6388	2006.27	2014.44	8.18
NGC1851	2006.33	2014.51	8.17	NGC6397	2006.41	2014.34	7.93
NGC2298	2006.45	2014.27	7.82	NGC6441	2006.41	2014.36	7.95
NGC2808	2006.17	2013.69	7.52	NGC6496	2006.31	2014.01	7.71
NGC3201	2006.20	2013.85	7.65	NGC6535	2006.25	2014.48	8.23
NGC4590	2006.18	2014.07	7.88	NGC6541	2006.25	2014.29	8.04
NGC4833	2006.57	2014.16	7.59	NGC6584	2006.40	2014.02	7.62
NGC5024	2006.17	2014.04	7.87	NGC6624	2006.29	2014.08	7.79
NGC5053	2006.18	2014.15	7.97	NGC6637	2006.39	2014.32	7.93
NGC5272	2006.14	2012.37	6.23	NGC6652	2006.40	2013.93	7.52
NGC5286	2006.17	2013.95	7.78	NGC6656	2006.25	2014.54	8.29
NGC5466	2006.28	2014.13	7.85	NGC6681	2006.39	2014.09	7.70
NGC5897	2006.27	2014.25	7.97	NGC6715	2006.40	2014.09	7.69
NGC5904	2006.20	2014.31	8.11	NGC6717	2006.24	2014.45	8.21
NGC5927	2006.28	2014.63	8.34	NGC6723	2006.42	2014.41	7.99
NGC5986	2006.29	2014.60	8.31	NGC6752	2006.40	2010.34	3.95
NGC6093	2006.27	2012.44	6.17	NGC6779	2006.36	2014.17	7.81
NGC6101	2006.42	2014.19	7.77	NGC6791	2004.74	2013.97	9.23
NGC6121	2006.18	2014.82	8.65	NGC6809	2006.30	2014.44	8.14
NGC6144	2006.29	2014.28	7.99	NGC6838	2006.36	2014.08	7.71
NGC6171	2006.25	2014.32	8.08	NGC6934	2006.25	2014.20	7.95
NGC6205	2006.25	2012.37	6.12	NGC6981	2006.38	2014.11	7.73
NGC6218	2006.17	2014.01	7.85	NGC7078	2006.33	2011.79	5.46
NGC6254	2006.18	2014.02	7.84	NGC7089	2006.29	2013.69	7.40
NGC6304	2006.29	2014.04	7.76	NGC7099	2006.34	2014.54	8.20
NGC6341	2006.28	2014.20	7.92				

try with the proper motions in the *Gaia* Data Release 2 (Gaia Collaboration et al. 2016a, 2018). However, the *Gaia* catalogue is severely incomplete near the core of GCs (see, e.g., Libralato et al. 2018), and furthermore most cluster stars are well below Gaia's faint limit. Therefore, in order to help interested users to select cluster members, we include in our photometric catalogues an estimate of the membership probability P_μ. In this section we will describe how we measured relative motions and estimated membership probabilities.

To compute relative PMs, we adopted the approach described in many previous publications by our group (see, e.g., Bedin et al. 2003; Anderson et al. 2006; Yadav et al. 2008; Bellini & Bedin 2010; Libralato et al. 2014; Nardiello et al. 2015; Libralato et al. 2015; Nardiello et al. 2016; Kerber et al. 2018). The routine KS2 provides raw catalogues, one for each exposure, containing positions and magnitudes of the stars listed in the final catalogue as measured on the single images. We used these raw catalogues to compute the relative PMs; for this computation we excluded F275W raw catalogues because of colour-dependent systematic effects in the geometric-distortion correction of this filter (Bellini et al. 2011)

We used six-parameter local transformations and a sample of likely cluster members (red-giant branch, RGB, sub-giant branch, SGB, and main sequence, MS, stars) to compute the displacement between the stellar positions in two different epochs. We started with a first, preliminary, sample of likely cluster members, selected on the $m_{\rm F814W}$ vs.

$(m_{\rm F606W} - m_{F814W})$ CMD, to compute the coefficients of the six-parameter linear transformations between the positions of the raw catalogues and the final catalogue. In order to minimise the effects of residual uncorrected geometric distortion, we computed the transformations using local samples (50 stars) of likely cluster members. Stars in each single-exposure catalogue of the first-epoch data set were compared to stars in each single-exposure catalogue of the second-epoch data set. Suppose we have N exposures for the first epoch and M exposures for the second epoch, then we end up with $N \times M$ displacements for each star. The computed relative proper motion of a star is the average of all these displacements along the X and the Y axes. The assigned error is simply the RMS of the displacement residuals around the average. Because the displacements are not statistically independent, the assigned errors are not a reliable estimate of the proper-motion errors, but can still be used to estimate membership probabilities (see Anderson et al. 2006 for an in-depth description of the method). We used these displacements to remove from the list of likely cluster members objects that had colours placing them close to the cluster sequences but had a field-star-like motion (i.e. those stars with proper motions relative to the cluster mean motion $> 6\,{\rm mas\,yr^{-1}}$). We iterated the procedure three times using the new member list to compute the improved linear transformations with each iteration.

KS2 does not measure the positions and fluxes of saturated stars. Therefore, we used the outputs of first pass
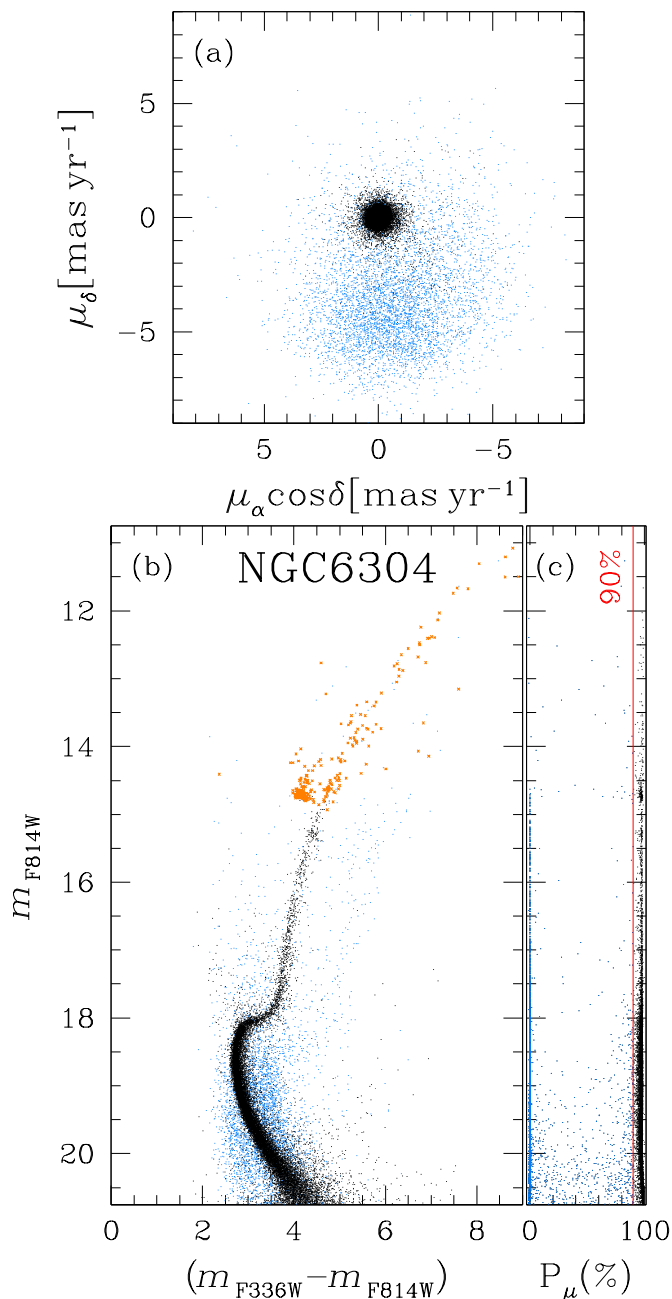
Figure 4. Likely NGC 6304 members selection. Panel (a) shows the VPD for the well-measured stars; panel (b) illustrates the m_{F814W} vs. $m_{F336W}-m_{F814W}$ CMD: in orange are the saturated stars in at least one filter; panel (c) is the membership probability as a function of the F814W magnitude. In all the plots we highlighted in azure the stars having $P_\mu < 90\%$ and in black the likely cluster members.

photometry to obtain the relative proper motions of these stars.

Since the coefficients of the six-parameter linear transformations are computed using likely cluster members, the stellar displacements are computed relative to the cluster mean motion, and therefore, in the vector-point diagram (VPD), cluster stars will be centred around (0,0), while field stars will lie in different regions of the VPD. The mean date

of the adopted observations for the first and second epoch and the time baseline are listed in Table 2.

Membership probabilities were then computed using the local-sample method, similarly to what was done in Bellini et al. (2009) and Libralato et al. (2014). For each target star, the membership probability is estimated using a sub-sample of reference 500 stars in the catalogue. These reference stars were initially chosen on the basis of PM error (typically ±0.25 mas yr^{-1}) and a magnitude similar to those of the target. The only exceptions are for target stars along the SGB and RGB, for which—due to small-number statistics—we considered as reference stars sources over the entire SGB-RGB sequence.

The cluster density function is modelled with an axisymmetric 2D Gaussian distribution centred on the origin of the VPD (since PMs are computed relative to the cluster's bulk motion). The sigma of the 2D Gaussian is magnitude dependent, and is defined as the 68.27th percentile of the $\sqrt{\mu_x^2 + \mu_y^2}$ distribution at any given magnitude. Field stars are assumed to have a flat distribution in the VPD, which is a fair assumption for the vast majority or our clusters. The remaining parameters of the local-sample method (see Eq. 10 of Kozhurina-Platais et al. 1995) are solved-for using least-squares techniques.

Figure 4 shows an example of field-star decontamination based on membership probabilities. Panels (a), (b), and (c) show the VPD, the m_{F814W} vs. $m_{F336W}-m_{F814W}$ CMD, and the membership distribution P_μ, respectively, for all the well-measured stars of NGC 6304: in black are the stars having a membership probability $P_\mu > 90\%$, in azure the other stars. In panel (b) we highlight in orange the stars that are saturated in at least one of the two filters.

Stars with unrealistic PM errors[4] are not considered in our membership-probability determination. This limits our ability to estimate membership-probabilities to stars brighter than a certain magnitude threshold that varies from cluster to cluster.

5 THE NEED FOR A NEW DATA RELEASE

In Paper VIII preliminary catalogues of the clusters in our project were released, in order to provide to the astronomical community an initial estimate of positions, luminosities, and colours of bright stars belonging to different populations in order to enable target selection for spectroscopic observations. As clearly stated in Paper VIII, this was the main purpose of the preliminary published catalogues.

The data-reduction pipelines used in this work and in Paper VIII are different. In the following, we list the most important improvements.

1) Perturbed PSFs: In Paper VIII static library PSFs were used. As explained in Sect. 2, in this work we perturbed library PSFs to take into account of spatial and temporal variations of the PSFs and to empirically reproduce the shape of the stars in each single image. This procedure was not adopted in Paper VIII;

---

[4] Stars with extremely (several sigmas) underestimated or overestimated PM errors with respect to those of stars with similar magnitude.
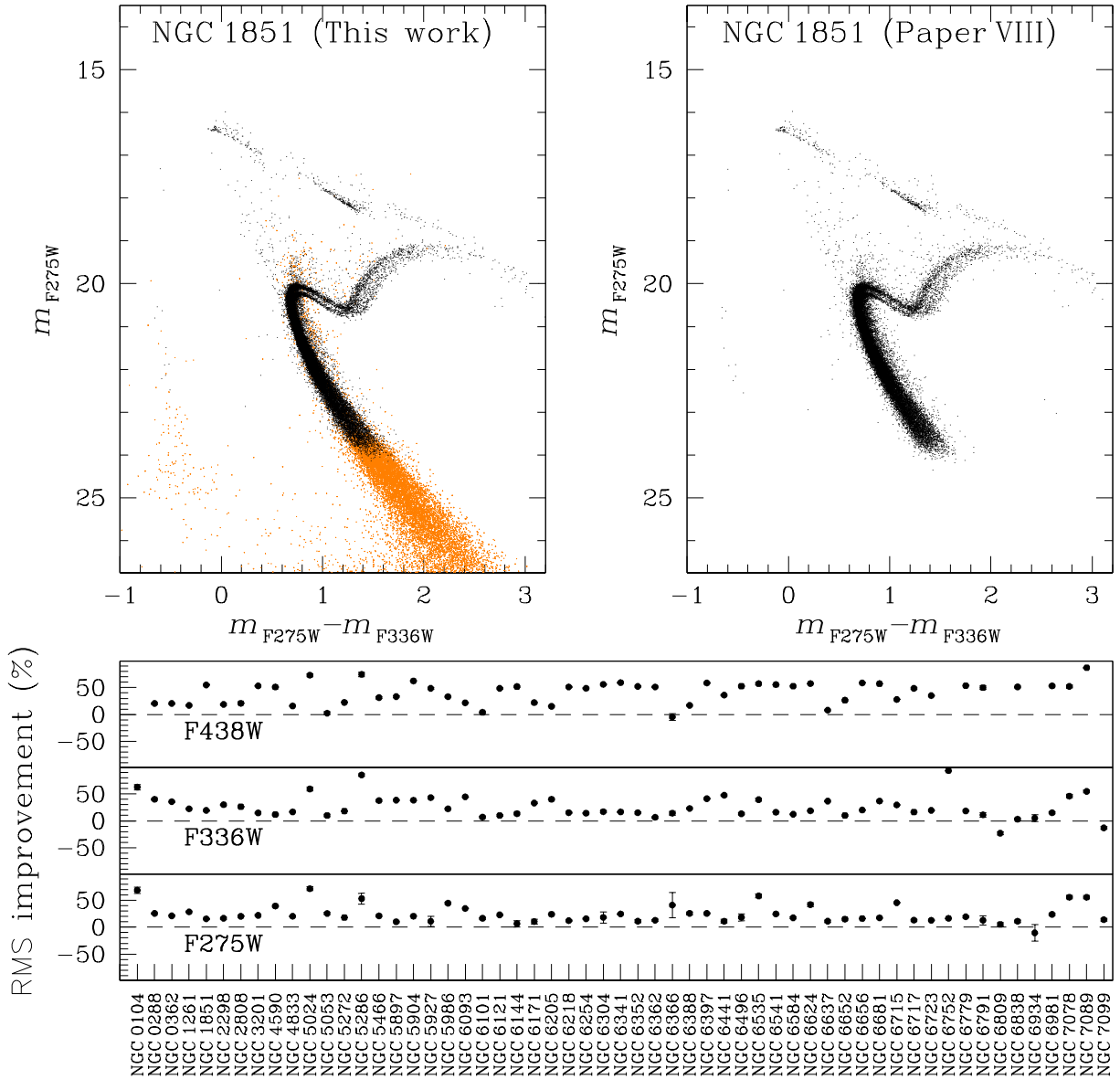
Figure 5. Comparison between catalogues of present work and Paper VIII. Top-panels show the m_{F275W} vs. $m_{F275W} - m_{F336W}$ CMDs of NGC 1851 obtained with the catalogue obtained in the present work (left-hand panel) and the Paper VIII catalogue (right-hand panel). Black points are the stars in common to the two data-release, orange points the stars measured in this work. Bottom panels show the photometric RMS improvements of our catalogues with respect to Paper VIII ones for F275W, F336W, and F438W bands.

2) Neighbour subtraction: For the present catalogue, when we measured the position and the flux of each source, we subtracted the neighbours to avoid the contamination by other close stars. This allowed us to better estimate the real flux of each star (as well as the measurement error), even in very crowded environments. In Paper VIII neighbour stars were not subtracted;

3) Faint stars: Because in Paper VIII we were interested only in measuring bright stars, only stars with S/N$\gtrsim$ 10 were searched in each image. The main consequence is that the faint part of the CMD was lacking in Paper VIII. In the present work we searched for each significant peak ($\geq 1\sigma$

above the sky) combining all the images, and measured the associated source using three different photometric methods.

4) Optical filters and UV completeness: In Paper VIII UV starlists were cross-identified with former ACS GCS catalogues (Sarajedini et al. 2007), and many bright stars in UV bands were lost. In the present work we also re-reduced data from the GO-10775 in an effort to improve the photometry in F606W and F814W bands using the new pipeline. Moreover, because we searched for stars using all filters, the new catalogues include stars bright in UV, even if they are too faint to be detected in optical bands (e.g., white dwarfs).

Figure 5 gives an example of the photometric improvements of the catalogues released by this work with respect to the preliminary catalogue in Paper VIII. The bottom panels show the RMS improvements (in percentage) of our photometry compared to that published in Paper VIII for the filters F275W, F336W, and F438W. The RMS was calculated for the stars in common between the two catalogues in the magnitude range $15 \leq m_X \leq 20$, with X=F275W, F336W, F438W. In this interval we computed the 3.5σ-clipped median and dispersion of RMS_X for both catalogues and calculated the value $100\times[1-RMS_X(\text{this work})/RMS_X(\text{Paper VIII})]$ that we used as indicator of photometric improvement. On average, our photometry has a ~20-30% lower RMS than that published in Paper VIII. Top panels of Fig. 5 illustrate a comparison between the m_{F275W} vs. $m_{F275W} - m_{F336W}$ CMDs of NGC 1851 from method-1 photometry (left panel) and the catalogue published in Paper VIII. In black we show the stars in common between these catalogues, in orange the stars measured in the present work, but missing in Paper VIII catalogue. The photometric improvement is evident, especially at the SGB and MS level.

Previous papers of the series are based on the catalogues described in Paper I, which were generated for internal use, and have not been published. Even though the routines used to obtain may be slightly different from the ones we adopted for the present paper, these catalogues were extracted using perturbed PSFs and neighbour subtraction. The F275W, F336W, and F438W photometric precision of this dataset and the internal-use set are comparable. The main difference regards the optical filters: as with the preliminary catalogue, the UV catalogues extracted in Paper I were cross-identified with pre-existing ACS GCS catalogues (Sarajedini et al. 2007) with all the limitations we discussed above for UV-bright sources. The catalogues we publish in this paper includes a new reduction of ACS GO-10775 F606W and F814W data, and includes UV and optical magnitudes of sources detected significantly in at least one of the F275W, F336W, F438W, F606W, and F814W bands.

6 THE DATA RELEASE

This new data release replaces the preliminary public available data release of Paper VIII (see Section 5). The new released material is part of the project "HST UV Globular cluster Survey" (HUGS). All of the data products from HUGS are available at Mikulski Archive for Space Telescopes (MAST, http://dx.doi.org/10.17909/T9810F) as a High Level Science Product.

We release the astro-photometric catalogues for all 57 clusters and, for each of them, we also release all the astrometrised stacked images (see Sect. 2 for details). The released material will be available at the "Exoplanets and Stellar Populations Group" (ESPG) website of the Università degli Studi di Padova, and on the MAST under the project HUGS[5].

For each cluster we release three catalogues, one for each photometric method. The catalogues contain information on the positions and on the photometry of each star found in the field. The catalogues also include membership probability. In Table 3 we describe the content of each column. The same description is also included in the header of each catalogue. For exemplification purpose, Table 4 show three rows of one of the released tables.

The catalogues that we make public here are complemented by the astrometric and photometric catalogues of the external ACS/WFC fields for 48 GCs plus NGC 6791 observed in parallel to the GO-13297 WFC3/UVIS central fields and published in Paper XIII. All catalogues are available at ESPG webpage

---

[5] https://archive.stsci.edu/prepds/hugs/

Table 3. Description of the column content of the astro-photometric catalogues.

Column	Name	Unit	Explanation
01,02	X, Y	[pix]	(x,y) stellar position in a reference system where the cluster center is in (5000,5000)
03	m_{F275W}	[mag]	F275W calibrated magnitude
04	RMS_{F275W}	[mag]	F275W photometric RMS
05	$QFIT_{F275W}$		F275W quality-fit parameter
06	$RADXS_{F275W}$		F275W sharp parameter
07	$N_{f,F275W}$		Number of F275W exposures the source is found [99: saturated star]
08	$N_{g,F275W}$		Number of F275W exposures the source is well measured [99: saturated star]
09	m_{F336W}	[mag]	F336W calibrated magnitude
10	RMS_{F336W}	[mag]	F336W photometric RMS
11	$QFIT_{F336W}$		F336W quality-fit parameter
12	$RADXS_{F336W}$		F336W sharp parameter
13	$N_{f,F336W}$		Number of F336W exposures the source is found [99: saturated star]
14	$N_{g,F336W}$		Number of F336W exposures the source is well measured [99: saturated star]
15	m_{F438W}	[mag]	F438W calibrated magnitude
16	RMS_{F438W}	[mag]	F438W photometric RMS
17	$QFIT_{F438W}$		F438W quality-fit parameter
18	$RADXS_{F438W}$		F438W sharp parameter
19	$N_{f,F438W}$		Number of F438W exposures the source is found [99: saturated star]
20	$N_{g,F438W}$		Number of F438W exposures the source is well measured [99: saturated star]
21	m_{F606W}	[mag]	F606W calibrated magnitude
22	RMS_{F606W}	[mag]	F606W photometric RMS
23	$QFIT_{F606W}$		F606W quality-fit parameter
24	$RADXS_{F606W}$		F606W sharp parameter
25	$N_{f,F606W}$		Number of F606W exposures the source is found [99: saturated star]
26	$N_{g,F606W}$		Number of F606W exposures the source is well measured [99: saturated star]
27	m_{F814W}	[mag]	F814W calibrated magnitude
28	RMS_{F814W}	[mag]	F814W photometric RMS
29	$QFIT_{F814W}$		F814W quality-fit parameter
30	$RADXS_{F814W}$		F814W sharp parameter
31	$N_{f,F814W}$		Number of F814W exposures the source is found [99: saturated star]
32	$N_{g,F814W}$		Number of F814W exposures the source is well measured [99: saturated star]
33	P_μ	[%]	Membership probability [-1.0: not available]
34	α	[deg.]	Right ascension (J2000, epoch 2015) of the star
35	δ	[deg.]	Declination (J2000, epoch 2015) of the star
36	ID		Identification number of the star
37	ITER		Iteration the star was found
			1-5: found in F814W and F606W images
			6: found in F438W images
			7: found in F336W images
			8: found in F275W images

Note: For NGC 0104 and NGC 6752, the F438W quantities are referred to the ACS/WFC F435W filter.

Table 4. Three lines from the catalogue of NGC 6304.

X	Y	m_{F275W}	RMS$_{F275W}$	QFIT$_{F275W}$	RADXS$_{F275W}$	N$_{f,F275W}$	N$_{g,F275W}$	m_{F336W}	RMS$_{F336W}$	QFIT$_{F336W}$	RADXS$_{F336W}$	N$_{f,F336W}$	N$_{g,F336W}$
6993.4438	2488.7637	24.0801	0.0000	0.7845	-0.4151	1	1	22.3862	0.0137	0.9844	0.0308	2	1
4117.0439	2489.3533	23.1821	0.0000	0.9453	-0.0596	1	1	21.4650	0.0103	0.9955	0.1101	2	1
4674.6870	2490.8945	-99.9999	99.9999	0.0000	9.9999	0	0	-99.9999	99.9999	0.0000	9.9999	0	0

m_{F438W}	RMS$_{F438W}$	QFIT$_{F438W}$	RADXS$_{F438W}$	N$_{f,F438W}$	N$_{g,F438W}$	m_{F606W}	RMS$_{F606W}$	QFIT$_{F606W}$	RADXS$_{F606W}$	N$_{f,F606W}$	N$_{g,F606W}$	m_{F814W}	RMS$_{F814W}$
21.3648	0.0000	0.9933	0.1235	1	1	19.5705	0.0025	1.0000	0.0013	4	1	18.4205	0.0027
21.1103	0.0000	0.9960	-0.0177	1	1	19.7744	0.0035	0.9999	0.0324	4	1	18.7334	0.0032
-99.9999	99.9999	0.0000	9.9999	0	0	19.9864	0.0000	0.9999	0.0615	1	1	18.9580	0.0000

QFIT$_{F814W}$	RADXS$_{F814W}$	N$_{f,F814W}$	N$_{g,F814W}$	P$_{\mu}$	α	δ	ID	ITER
1.0000	0.0049	4	1	00.0	258.638467	-29.489565	R0000287	1
1.0000	0.0595	4	1	98.1	258.638913	-29.489539	R0000288	1
0.9999	0.0999	1	1	-01.0	258.614414	-29.489541	R0000289	1

REFERENCES

Anderson J., Bedin L. R., 2010, PASP, 122, 1035

Anderson J., King I. R., 2006, Technical report, PSFs, Photometry, and Astronomy for the ACS/WFC

Anderson J., Bedin L. R., Piotto G., Yadav R. S., Bellini A., 2006, A&A, 454, 1029

Anderson J., et al., 2008, AJ, 135, 2055

Bastian N., 2015, preprint, (arXiv:1510.01330)

Bastian N., Lardo C., 2018, Annual Review of Astronomy and Astrophysics, 56

Bedin L. R., Piotto G., King I. R., Anderson J., 2003, AJ, 126, 247

Bedin L. R., King I. R., Anderson J., Piotto G., Salaris M., Cassisi S., Serenelli A., 2008, ApJ, 678, 1279

Bedin L. R., Salaris M., Piotto G., Anderson J., King I. R., Cassisi S., 2009, ApJ, 697, 965

Bedin L. R., Salaris M., King I. R., Piotto G., Anderson J., Cassisi S., 2010, ApJ, 708, L32

Bellini A., Bedin L. R., 2009, PASP, 121, 1419

Bellini A., Bedin L. R., 2010, A&A, 517, A34

Bellini A., et al., 2009, A&A, 493, 959

Bellini A., Anderson J., Bedin L. R., 2011, PASP, 123, 622

Bellini A., et al., 2014, ApJ, 797, 115

Bellini A., Anderson J., Bedin L. R., King I. R., van der Marel R. P., Piotto G., Cool A., 2017, ApJ, 842, 6

Bellini A., et al., 2018, ApJ, 853, 86

Bohlin R. C., 2016, AJ, 152, 60

Deustua S. E., Mack J., Bajaj V., Khandrika H., 2017, Technical report, WFC3/UVIS Updated 2017 Chip-Dependent Inverse Sensitivity Values

Dressel L., 2018, Wide Field Camera 3 Instrument Handbook, Version 10.0

Gaia Collaboration et al., 2016a, A&A, 595, A1

Gaia Collaboration et al., 2016b, A&A, 595, A2

Gaia Collaboration et al., 2018, A&A, 616, A1

Gilliland R. L., 2004, Technical report, ACS CCD Gains, Full Well Depths, and Linearity up to and Beyond Saturation

Gilliland R. L., Rajan A., Deustua S., 2010, Technical report, WFC3 UVIS Full Well Depths, and Linearity Near and Beyond Saturation

Goldsbury R., Richer H. B., Anderson J., Dotter A., Sarajedini A., Woodley K., 2010, AJ, 140, 1830

Kerber L. O., Nardiello D., Ortolani S., Barbuy B., Bica E., Cassisi S., Libralato M., Vieira R. G., 2018, ApJ, 853, 15

Kozhurina-Platais V., Girard T. M., Platais I., van Altena W. F., Ianna P. A., Cannon R. D., 1995, AJ, 109, 672

Libralato M., Bellini A., Bedin L. R., Piotto G., Platais I., Kissler-Patig M., Milone A. P., 2014, A&A, 563, A80

Libralato M., et al., 2015, MNRAS, 450, 1664

Libralato M., et al., 2018, ApJ, 861, 99

Marino A. F., et al., 2018, ApJ, 859, 81

Milone A. P., et al., 2012, A&A, 540, A16

Milone A. P., et al., 2017, MNRAS, 464, 3636

Nardiello D., Milone A. P., Piotto G., Marino A. F., Bellini A., Cassisi S., 2015, A&A, 573, A70

Nardiello D., Libralato M., Bedin L. R., Piotto G., Ochner P., Cunial A., Borsato L., Granata V., 2016, MNRAS, 455, 2337

Nardiello D., et al., 2018, MNRAS, 477, 2004

Piotto G., et al., 2015, AJ, 149, 91

Renzini A., et al., 2015, MNRAS, 454, 4197

Sarajedini A., et al., 2007, AJ, 133, 1658

Simioni M., et al., 2018, MNRAS, 476, 271

Soto M., et al., 2017, AJ, 153, 19

Yadav R. K. S., et al., 2008, A&A, 484, 609

This paper has been typeset from a TeX/LaTeX file prepared by the author.